

Substrate-Dependent Hydridic and Radical Reactivity of Triiron Hydride Clusters

Brian J. Knight, Kevin J. Anderton, Juan F. Torres, Vincent J. Catalano, Ricardo Garcia-Serres, and Leslie J. Murray*



Cite This: *Inorg. Chem.* 2025, 64, 8052–8063



Read Online

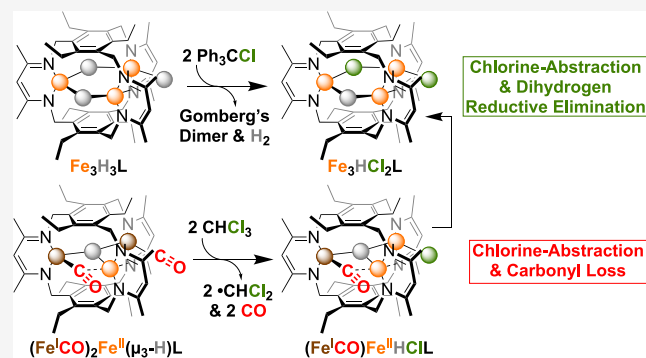
ACCESS |

Metrics & More

Article Recommendations

Supporting Information

ABSTRACT: The reactivity of iron clusters with one of more μ -hydrides and in the weak field pertains to catalysis on surfaces and biological metal cluster cofactors. As a model, then, a reactivity survey of the weak-field ligated iron hydride clusters $\text{Fe}_3\text{H}_3\text{L}$ (1) and $(\text{FeCO})_2\text{Fe}(\mu_3\text{-H})\text{L}$ (2) (where L^{3-} is a tris(β -diketiminato)-cyclophanate) with Brønsted acids, organochlorides, acetyl chloride, boron trihalides, and titanium electrophiles is reported. Complex 1 reacts with Brønsted acids H_2O and $[\text{Et}_3\text{NH}][\text{Cl}]$ to afford $\text{Fe}_3(\text{OH})_3\text{L}$ (3) and $\text{Fe}_3\text{H}_2\text{CIL}$ (4), respectively, consistent with hydridic reactivity. Clusters 1 and 2 react readily with organochlorides, such as CCl_4 , CHCl_3 , and CH_2Cl_2 , with identified intermediates supporting a radical pathway. Complex 1 reacts with trityl chloride (2 equiv) to selectively afford $\text{Fe}_3\text{HCl}_2\text{L}$ (5) with reductive elimination of dihydrogen observed. Mixed-valent complex 2 reacts with AcCl to afford $(\text{FeCO})\text{Fe}_2\text{HCIL}$ (9). The scope of reactivity displayed implicates possible pathways accessible to larger clusters in biology or on metal surfaces.



INTRODUCTION

Transition metal hydrides display broad reactivity, which is influenced by many factors such as bridging modes, oxidation state, and supporting ligands.^{1–5} As a consequence, transition metal hydrides are utilized in many societally important transformations, including production of hydrocarbon fuels,⁶ commodity chemicals,⁷ and fertilizers.⁸ Similarly, discrete mononuclear metal hydrides have been extensively investigated, with molecular compounds employed in energy storage,⁹ electrocatalysis,¹⁰ and chemical synthesis.^{11–13} Uniquely, however, polynuclear metal species or clusters with bound hydride ligands can serve as models to study the structure and reactivity of metal hydride surfaces and clusters in heterogeneous^{14,15} and metalloenzyme systems.^{16–18} Iron hydride clusters are of particular interest given the preponderance of iron surfaces and clusters in catalytic systems that rely on metal-hydrides. Historically, synthetic clusters are supported by strong field donors (e.g., CO and phosphines), and these compounds exhibit well-described protic or hydridic behavior for the bound hydride.^{19–23} However, the local spin states of metal centers influence the reactivity and can afford radicaloid character on ligands or thermal access to low lying electronic states with lower activation barriers, termed spin acceleration.^{24–28} The consequence of spin-state and hydride bridging modes—especially in polynuclear compounds—on reactivity then remains an ongoing research focus.

Biological cofactors, such as FeMoco, have received considerable attention toward understanding the breadth of iron-hydride cluster reactivity. Investigations into the contribution of catalytically relevant ligands (e.g., C- or S-based ligands) on this reactivity are typically limited to complexes with low-spin electronic configurations, resulting in archetypical hydridic behavior.²⁹ However, the more electronically analogous weak-field ligated $[\text{Fe}_2(\mu\text{-H})_2]^{2+}$ dinuclear species in Figure 1A illustrate reductive elimination and H atom and hydride transfer reactivity.^{30–33} However, many of these complexes exist as a monomer–dimer equilibrium in solution, limiting conclusions on the role of the dinuclear assembly in the reactivity.³⁴ Model systems that prevent cluster dissolution would then be more relevant to those found on metal surfaces or in biological cofactors. Additionally, such polynuclear metal hydride complexes allow one to investigate the factors, such as spin state, cluster oxidation state, and bridging modes, that modulate hydride ligand reactivity and character (Figure 1B).

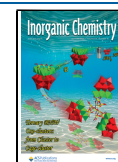
Our group reported a tris(β -diketiminato) cyclophane ligand (L^{3-}) to stabilize low-coordinate trimetallic clusters in a weak

Received: January 6, 2025

Revised: April 8, 2025

Accepted: April 11, 2025

Published: April 16, 2025



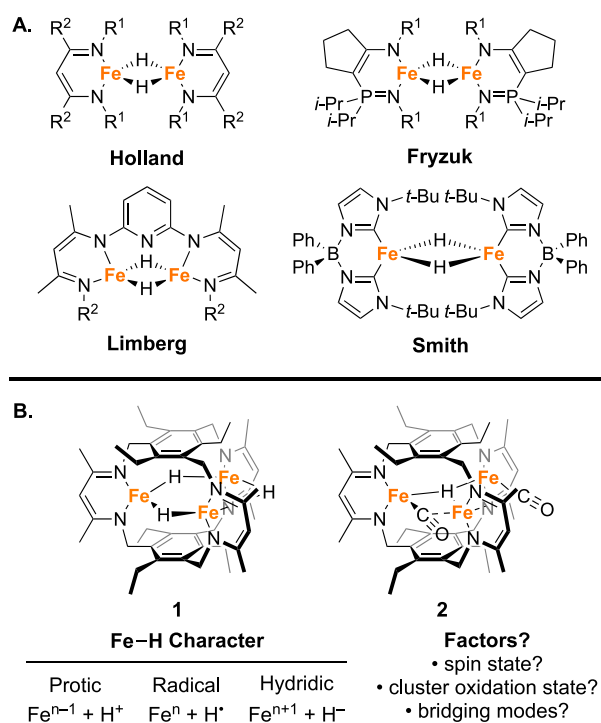


Figure 1. (A) Synthetic iron clusters containing weak-field ligands and bridging hydrides. (B) Potential factors affecting hydride character (i.e., protic, radical, hydridic) of 1 and 2.

ligand field.^{35–38} Specific to iron hydride clusters, Lee et al. have previously reported hydride transfer from $\text{Fe}_3\text{H}_3\text{L}$ (1) to CO_2 , followed by more detailed kinetic studies from Hong and Murray.^{39,40} Anderton et al. later observed H_2 reductive elimination in reaction with CO to yield $(\text{FeCO})_2\text{Fe}(\mu_3\text{-H})\text{L}$ (2).⁴¹ In alignment with our kinetic data, we postulate that these hydride ligands are coordinatively fluxional with a low energy barrier to interconversion between terminal and bridging modes. As part of delineating the factors governing hydride fluxionality, migratory insertion vs reductive elimination, and other possible reactivity manifolds, we report here the reactivity of 1 and 2 with various electrophiles and Lewis acids. In particular, organochlorides were evaluated, due to their availability, variety, and differential reaction kinetics, to investigate the reaction mechanism and access multiple product outcomes. These studies, including reaction with a radical clock substrate, point to an accessible radical reaction pathway for these complexes, leading to net hydrogen-atom loss and adding to the previously observed insertion and reductive elimination pathways.

EXPERIMENTAL METHODS

General Considerations. All operations were performed under a dry, air-free atmosphere using an argon-filled MBraun Unilab glovebox, dinitrogen-filled Innovative Technologies glovebox, or standard Schlenk techniques. Tetrahydrofuran (THF), benzene, toluene, *n*-hexane, and *n*-pentane were purchased from Sigma-Aldrich, then purified through drying columns from Innovative Technologies solvent purification system and stored over activated 3 Å molecular sieves. The water content of each solvent was measured using a Mettler Toledo C20 Coulometric Karl Fischer Titrator prior to use and was below 1 ppm in all cases. Celite and 3Å molecular sieves were dried at 220 °C under vacuum overnight. CO (UHP

grade, 99.9%) was purchased from Airgas, Inc. and purified by passage through two cold traps (liquid N_2 /*i*-PrOH). ^{13}C O was purchased from Sigma-Aldrich and used as received. The organochlorides and TMSCl were distilled over CaH_2 prior to use. $[\text{Et}_3\text{NH}][\text{Cl}]$ was dried under high-vacuum with a P_2O_5 trap for at least 1 d. All other reagents were purchased from Sigma-Aldrich and used without purification. Both KBHET_3 and LiDBET_3 were prepared from equimolar amounts of BEt_3 and potassium hydride/deuteride in toluene and hexanes, which was crystallized at -34 °C from the still biphasic mixture. Deuterated solvents were purchased from Sigma-Aldrich or Cambridge Isotope Laboratories, dried using the following methods, and stored over 3 Å molecular sieves. THF- d_8 was stirred with Na/benzophenone for 2 h at 55 °C and distilled under argon. Benzene- d_6 and toluene- d_8 were heated at reflux overnight in the presence of CaH_2 , distilled, and degassed using three cycles of freeze–pump–thaw (20 mTorr). CDCl_3 was used as purchased. ^1H Nuclear Magnetic Resonance (^1H NMR) spectra were recorded on a Varian Inova 500 MHz spectrometer or a Mercury 300 MHz spectrometer. Chemical shifts were reported in δ (ppm) and were referenced to solvent resonances $\delta\text{H} = 7.16$ ppm for benzene- d_6 , $\delta\text{H} = 2.08$ or 6.98 ppm for toluene- d_8 , $\delta\text{H} = 3.58$ ppm for THF- d_8 , and $\delta\text{H} = 7.26$ ppm for CDCl_3 . One NMR experiment was conducted in standard THF (not deuterium-labeled). The experiment parameters were D1 = 0 s, O1P = 0 ppm, SW = 499.75 ppm, TD = 131072, AQ = 0.32768 s, P1 = 9.7 s, L30 = 2, O2P = 77.000 ppm, ISW = 499.75 ppm, and 1TD = 131072. FT-IR spectra were collected on drop-casted samples using a ThermoFisher Scientific Nicolet iS5 spectrometer equipped with an iD7 ATR stage and using the OMNIC software package at 1.0 cm^{-1} resolution and 32 scans per sample. Solution magnetic susceptibilities were determined by the Evans method.^{89–92} Samples for UV/visible spectroscopy were prepared under an Ar atmosphere using air-free anhydrous THF, transferred to airtight cuvettes (Starna quartz cells, Atascadero, CA, USA), and spectra were recorded using an Agilent Cary 50 spectrophotometer. Mass spectrometry data were collected using an Agilent 6220 ESI-TOF on samples prepared in anhydrous THF. Elemental analysis (CHN) was determined on a PerkinElmer 2400 Series II Analyzer, with the weights of the samples measured on a PerkinElmer Model AD6000 Autobalance and performed at the Center for Enabling New Technologies Through Catalysis (University of Rochester, NY). Mössbauer samples were ground into fine powders and placed in Delrin containers. Mössbauer spectra were measured on a low-field Mössbauer spectrometer equipped with a closed-cycle SHI-850–5 cryostat from Janis and SHI or on a high-field spectrometer equipped with an Oxford Instruments Spectromag 4000 cryostat containing an 8 T split-pair superconducting magnet. The spectrometers were operated in constant acceleration mode in transmission geometry. The isomer shifts are referenced against a rt metallic iron foil. Analysis of the data was performed using the in-house developed Python package easyMoss.⁹³ Low-temperature X-ray diffraction data for $\text{Fe}_3(\text{OH})_3\text{L}$ (3) was collected Bruker Apex II single crystal diffractometer.

Synthetic Procedures and Characterization of Compounds. $\text{Fe}_3\text{H}_3\text{L}$ (1). Prepared as previously reported.³⁹ ^1H NMR (500 MHz, benzene- d_6): δ 79.79 (12H), -0.59 (3H), -6.91 (18H), -19.57 (18H), -44.51 (12H).

$\text{Fe}_3\text{D}_3\text{L}$ (1-D). Prepared as previously reported.⁴¹

(FeCO)₂Fe(μ₃-H)L (2). Prepared as previously reported.⁴¹ ¹H NMR (500 MHz, toluene-*d*₆): δ 161.81 (4H), 78.11 (4H), 59.98 (4H), 5.62 (4H), 3.96 (6H), -3.55 (12H), -14.01 (4H), -17.60 (12H), -29.92 (4H), -35.36 (2H), -54.82 (1H), -57.14 (6H). ATR-IR (cm⁻¹): 1846 (ν_{CO}).

(FeCO)₂Fe(μ₃-H)L (2-¹³CO). Prepared as previously reported. ATR-IR (cm⁻¹): 1804 (ν_{CO}).⁴¹

(FeCO)₂Fe(μ₃-D)L (2-D). Prepared as previously reported, but with Fe₃D₃L (1-D) instead of Fe₃H₃L (1) as a starting material.⁴¹ ¹H NMR (500 MHz, toluene-*d*₆): δ 161.44 (4H), 77.64 (4H), 59.70 (4H), 5.48 (4H), 3.91 (6H), -3.52 (12H), -13.97 (4H), -17.49 (12H), -29.72 (4H), -35.10 (2H), -54.93 (1H), -57.04 (6H). ATR-IR (cm⁻¹): 1879 (ν_{CO}), 1845 (ν_{CO}).

Fe₃(OH)₃L (3). A solution of Fe₃H₃L (1, 100 mg, 116 μmol) and H₂O (351 μL, 1.0 M in THF, 351 μmol) in toluene (12.0 mL) was heated and stirred at 90 °C for 3.5 d slowly changing the reaction from red to an amber yellow solution. The reaction was filtered through a toluene-rinsed Celite plug and then concentrated to an amber solid. The residue was recrystallized from a 90 °C toluene solution slowly cooled to -34 °C to afford the product (63.2 mg, 60% yield) as a large orange crystalline solid. This material was suitable for X-ray diffraction. ¹H NMR (500 MHz, benzene-*d*₆): δ 80.81 (12H), 2.11 (12H), 1.60 (18H), -3.43 (18H), -26.75 (3H). μ_{eff} (toluene-*d*₈, 298 K) = 6.6 μ_B. ATR-IR (cm⁻¹): 3642 (ν_{OH}), 1518, 1395, 1370, 1322, 1013, 727, 692. UV-vis (THF; nm (ε, mM⁻¹cm⁻¹)): 269 (1.6(1) × 10⁴), 332 (1.32(1) × 10⁴), 374 (2.50(3) × 10⁴), 384 (2.03(1) × 10⁴), 392 (1.86(1) × 10⁴). HRMS (ESI+) *m/z* calcd for (M+H₂O)⁺ [C₄₅H₆₆Fe₃N₆O₃+H₃O]⁺: 923.3267, found 923.3498. Anal. Found (calcd) for C₄₅H₆₆Fe₃N₆O₃(C₇H₈)_{0.7}: C, 61.86 (61.72); H, 7.35 (7.43); N, 8.58 (8.65).

Fe₃H₂ClL (4). In a scintillation vial, a solution of a 5.9:1 mixture of Fe₃H₂(O₂CH)L/Fe₃H(O₂CH)₂L (7/8, 83.1 mg, 78.2 μmol) in benzene (8.0 mL) was charged with TMSCl (100 μL, 788 mmol) at ambient temperature and left without stirring. The solution changed from orange to reddish orange. After 2 d, reddish orange crystals appeared. The solution was removed by a pipet and the crystals were dried under reduced pressure to afford the product (42.0 mg, 60% yield). ¹H NMR (500 MHz, benzene-*d*₆): δ = 134.14 (4H), 119.05 (4H), 108.08 (4H), -3.15 (10H; 6H+4H), -7.02 (12H), -31.23 (6H), 31.44 (2H), -31.99 (12H), -38.43 (4H), -54.16 (4H), (note: the peak integrating to 1H could not be identified with confidence). μ_{eff} (toluene-*d*₈, 298 K) = 6.2 μ_B. ATR-IR (cm⁻¹): 1517, 1435, 1428, 1393, 1374, 1332, 1015, 737.

Fe₃HCl₂L (5), procedure 1. In a scintillation vial with a Teflon stir bar, a suspension of (FeCO)₂Fe(μ₃-H)L (2, 60.0 mg, 65.7 μmol) in toluene (19 mL) was charged with a solution of TiCl₄ (1.00 mL, 65.7 mM in toluene, 65.7 μmol) at ambient temperature and stirred for 16 h. The reaction was filtered through a toluene-rinsed Celite plug and then concentrated to an amber solid. The residue was recrystallized from a 90 °C toluene solution slowly cooled to -34 °C to afford the product (12.0 mg, 14:1 Fe₃HCl₂L (5)/Fe₃(μ-Cl)₃L (6), 18% yield) as large red crystals. ¹H NMR (500 MHz, toluene-*d*₆): δ = 170.05 (4H), 148.86 (4H), 144.16 (4), 27.45 (6H), 24.28 (4), 0.61 (12H), -7.00 (6H), -8.19 (4), -44.82 (4H), -53.92 (12H) (note: the peaks integrating to 1H and 2H could not be identified with confidence). ATR-IR (cm⁻¹): 1519, 1456, 1428, 1395, 1371, 1326, 1068, 1015. μ_{eff} (toluene-*d*₈, 298 K) = 7.2 μ_B. UV-vis (THF; nm (ε, mM⁻¹cm⁻¹)): 327

(2.73(6) × 10⁴), 400 (4.8(2) × 10³), 420 (6.0(3) × 10³), 551 (2.9(6) × 10³). HRMS (ESI+) *m/z* calcd for (M+O)⁺ [C₄₅H₆₄Cl₂Fe₃N₆+O]⁺: 942.2561, found 942.2778.

Fe₃HCl₂L (5), Procedure 2. A solution of trityl chloride (20.5 mg, 73.0 μmol) in THF (2.0 mL) was added to a solution of Fe₃H₃L (1, 30.0 mg, 35.0 μmol) in THF (4.0 mL). The reaction mixture was stirred at ambient temperature for 2 h, then the volatiles were removed under reduced pressure. The residue was stirred with pentane (6.0 mL) for 1 h, and the solid collected by filtration. The bright orange powder was washed with pentane (2 × 2.0 mL) and dried under reduced pressure to yield the desired product (24.3 mg, 75% yield). Note: The yield was determined by the bulk mass of the material. Given that this material is not spectroscopically pure, the actual yield is less than 75%.

Fe₃Cl₃L (6). Prepared as previously reported.³⁶ ¹H NMR (500 MHz, benzene-*d*₆): δ 182.83 (12H), -7.98 (18H), -13.97 (12H), -43.13 (18H), -51.74 (3H).

Fe₃H₂(O₂CH)L (7) and Fe₃H(O₂CH)₂L (8). Prepared as previously reported.³⁹ Fe₃H₂(O₂CH)L (7) has previously been synthesized and characterized, while Fe₃H(O₂CH)₂L (8) was consistently observed as a minor impurity in the crude ¹H NMR spectrum of Fe₃H₂(O₂CH)L. Representative peaks of a ~6:1 crystalline mixture of Fe₃H₂(O₂CH)L/Fe₃H(O₂CH)₂L. Fe₃H₂(O₂CH)L - ¹H NMR (500 MHz, benzene-*d*₆): δ 147.08 (4H), 131.50 (4H), 86.55 (4H), -3.38 (6H), -7.06 (12H), -25.25 (6H), -36.15 (12H). Fe₃H(O₂CH)₂L - ¹H NMR (500 MHz, benzene-*d*₆, representative peaks): δ 135.09, 60.98.

(FeCO)Fe₂HClL (9). In a scintillation vial with a Teflon stir bar, a suspension of (FeCO)₂Fe(μ₃-H)L (2, 120 mg, 131 μmol) in toluene (19 mL) was charged with a solution of AcCl (1.00 mL, 131 mM in toluene, 131 μmol) at ambient temperature and stirred for 48 h. A small aliquot was concentrated and analyzed by ¹H NMR. The spectrum indicated residual starting material. After 3 d, three additional portions of AcCl (3 × 100 μL, 3 × 131 mM, 3 × 13.1 μmol) were added to the reaction every 2 d. The total AcCl added to the reaction was 1.3 equiv (170 μmol). The reaction solution was filtered through a toluene-rinsed Celite plug and concentrated to 10 mL. The remaining solvent was removed by slow evaporation with a vial of mineral oil to afford the crude product as an amber solid (80.5 mg, 67% yield). ¹H NMR (500 MHz, benzene-*d*₆): δ = 172.97 (2H), 144.12 (2H), 124.98 (2H), 109.99 (2H), 107.96 (2H), 78.81 (2H), 1.56 (6H), -8.12 (6H), -13.48 (6H), -28.80 (6H), -34.82 (6H), -41.06 (6H), (note: the remaining peaks could not be identified with confidence). ATR-IR (cm⁻¹): 1850 (ν_{CO}), 1521, 1431, 1394, 1334, 1016, 728. HRMS (ESI+) *m/z* calcd for (M+H)⁺ [C₄₆H₆₄ClFe₃N₆O+H]⁺: 920.2885, found 920.2951.

(FeCO)Fe₂DCIL (9-D). The synthesis followed the reported procedure for (FeCO)Fe₂HClL (9), but with (FeCO)₂Fe(μ₃-D)L (2-D) instead of (FeCO)₂Fe(μ₃-H)L (2) as a starting material. HRMS (ESI+) *m/z* calcd for (M+H)⁺ [C₄₆H₆₃DCIFe₃N₆O + H]⁺: 921.3024, found 921.2971.

(Fe¹³CO)Fe₂HClL (9-¹³CO). The synthesis followed the above procedure for (FeCO)Fe₂HClL (9), but with (Fe¹³CO)₂Fe(μ₃-H)L (2-¹³CO) instead of (FeCO)₂Fe(μ₃-H)L (2) as a starting material. ATR-IR (cm⁻¹): 1807 (ν_{CO}). HRMS (ESI+) *m/z* calcd for (M+H)⁺ [C₄₅¹³CH₆₄ClFe₃N₆O+H]⁺: 921.2841, found 921.2985.

$\text{Fe}_3\text{F}_3\text{L}$ (10). May be prepared as previously reported.⁴¹ ^1H NMR (toluene- d_6): δ 149.46 (12H), -13.04 (18H), -21.76 (3H), -39.01 (12H), -55.60 (18H).

Cyclopropane 12. Prepared as previously reported.⁵⁸

Reactivity Data. Detection of $\text{Fe}_3\text{H}_2\text{CIL}$ (4) and $\text{Fe}_3\text{HCl}_2\text{L}$ (5) from the Reaction of $\text{Fe}_3\text{H}_3\text{L}$ (1) and $[\text{Et}_3\text{NH}][\text{Cl}]$. In a scintillation vial with a Teflon stir bar, a solution of $\text{Fe}_3\text{H}_3\text{L}$ (1, 60.0 mg, 70.0 μmol) in THF (7.0 mL) was charged with $[\text{Et}_3\text{NH}][\text{Cl}]$ (38.5 mg, 280 μmol) and stirred at 45 °C for 4 d. Then, the reaction mixture was concentrated under reduced pressure. The residue was dissolved in benzene (20 mL), filtered through a plug of benzene-rinsed Celite, and the resulting solution was lyophilized. ^1H NMR analysis of the crude reaction mixture indicated a 4:1 mixture of $\text{Fe}_3\text{H}_2\text{CIL}$ (4)/ $\text{Fe}_3\text{H}_3\text{L}$ (1). Prolonged heating under these conditions produced an insoluble black material and $\text{Fe}_3\text{HCl}_2\text{L}$ (5).

Synthesis of $\text{Fe}_3\text{H}_2\text{CIL}$ (4) and $\text{Fe}_3\text{HCl}_2\text{L}$ (5) from the Reaction of $\text{Fe}_3\text{H}_2(\text{O}_2\text{CH})\text{L}$ (7) and $\text{Fe}_3\text{H}(\text{O}_2\text{CH})_2\text{L}$ (8) with TMSCl. A 200 mL Schlenk flask was charged with $\text{Fe}_3\text{H}_3\text{L}$ (1, 725 mg, 844 μmol), a Teflon-coated stir bar, and THF (120 mL). The solution was degassed by freeze–pump–thaw method and then exposed to a slow flow of CO_2 for ~ 1 h with stirring. The flask was closed and was stirred for an additional 24 h at ambient temperature. After this time, the reaction was evaporated and brought into an Ar-filled glovebox. A ^1H NMR was recorded in benzene- d_6 , and analysis of the crude material at this point indicated a $\sim 5:1$ ratio of $\text{Fe}_3\text{H}_2(\text{O}_2\text{CH})\text{L}$ (7)/ $\text{Fe}_3\text{H}(\text{O}_2\text{CH})_2\text{L}$ (8). The residue was redissolved in THF (72 mL), charged with TMSCl (134 μL , 1.44 mmol), and stirred for 41 h at ambient temperature. Analysis of the crude material at this point by IR spectroscopy indicated full consumption of the initially generated formate-containing product due to the disappearance of all stretches between 1676 and 1642 cm^{-1} . A ^1H NMR spectrum was recorded in toluene- d_8 indicating a $\sim 5:1$ ratio of $\text{Fe}_3\text{H}_2\text{CIL}$ (4)/ $\text{Fe}_3\text{HCl}_2\text{L}$ (5) and the formation of TMSO_2CH .

Synthesis of TMSO_2CH as an NMR Standard. A J. Young tube was charged with benzene- d_6 (400 μL), TMSCl (2.3 μL , 18.2 μmol), and then NaO_2CH (12.4 mg, 182 μmol). The tube was closed, inverted, and then sonicated in a 40 °C bath. After 2 h, a ^1H NMR spectrum was recorded, and TMSO_2CH was observed. ^1H NMR (benzene- d_6): δ = 7.69 (s, 1H), 0.14 (s, 9H).

Reaction of a 1:1 Mixture of $\text{Fe}_3\text{H}_3\text{L}$ (1) and $\text{Fe}_3\text{D}_3\text{L}$ (1-D) with CCl_4 . A J. Young NMR tube was charged with $\text{Fe}_3\text{H}_3\text{L}$ (1, 1.0 mg, 1.17 μmol), $\text{Fe}_3\text{D}_3\text{L}$ (1-D, 1.0 mg, 1.17 μmol), benzene- d_6 (400 μL), and then an CCl_4 (0.206 μL , 2.33 μmol) at ambient temperature. The tube was closed, inverted, and shaken. A ^1H NMR spectrum was recorded at 1 h indicating the formation of $\text{Fe}_3\text{HCl}_2\text{L}$ (5).

Detection of Intermediates in the Reaction of $\text{Fe}_3\text{H}_3\text{L}$ (1) with Organohalides. A J. Young NMR tube was charged with $\text{Fe}_3\text{H}_3\text{L}$ (1, 2.0 mg, 2.33 μmol), benzene- d_6 (400 μL), and then an organohalide (9.32 μmol) at ambient temperature. The tube was closed, inverted, and shaken. A ^1H NMR spectrum was typically recorded at 1, 12, 24, and 48 h.

Detection of CH_2Cl_2 in the Reaction of $\text{Fe}_3\text{H}_3\text{L}$ (1) with CHCl_3 . A J. Young NMR tube was charged with $\text{Fe}_3\text{H}_3\text{L}$ (1, 2.0 mg, 2.33 μmol), benzene- d_6 (400 μL), and then CHCl_3 (5.6 μL , 46.6 μmol) at ambient temperature. The tube was closed, inverted, and shaken. The mixture slowly changed from light brown to a slight orange. After 2 d, the volatiles were then

transferred to a second J. Young tube. A ^1H NMR spectrum was recorded in benzene- d_6 , and CH_2Cl_2 was detected.

Detection of CHDCl_2 and CH_2Cl_2 in the Reaction of $\text{Fe}_3\text{D}_3\text{L}$ (1-D) with CHCl_3 . A J. Young NMR tube was charged with $\text{Fe}_3\text{D}_3\text{L}$ (1-D, 2.0 mg, 2.33 μmol), benzene- d_6 (400 μL), and then CHCl_3 (0.75 μL , 9.32 μmol) at ambient temperature. The tube was closed, inverted, and shaken. The mixture slowly changed from light brown to a slight orange. After 2 d at ambient temperature, and the volatiles were then transferred to a second J. Young tube. A ^1H NMR spectrum was recorded in benzene- d_6 , and a 2:1 ratio of $\text{CHDCl}_2/\text{CH}_2\text{Cl}_2$ was detected.

Detection of Dichloroalkene (13) in the Reaction of $\text{Fe}_3\text{D}_3\text{L}$ (1-D) with Cyclopropane (12) in THF. A scintillation vial was charged with $\text{Fe}_3\text{D}_3\text{L}$ (1-D, 12.1 mg, 14.0 μmol), a Teflon-coated stir bar, and THF (2.4 mL), and then cyclopropane 12 (4.0 mg, 14.0 μmol) at ambient temperature. The vial was sealed with a Teflon-lined cap and stirred at ambient temperature. After 2 d, the mixture was filtered through a plug of THF-rinsed Celite and the filtrate was concentrated under reduced pressure. ^1H NMR analysis of the crude reaction mixture indicated that cyclopropane 12 had been converted to dichloroalkene 13. There was no deuterium enrichment in the product.

Detection of Gomberg's Dimer and Dihydrogen in the Reaction of $\text{Fe}_3\text{H}_3\text{L}$ (1) with Trityl Chloride. In a J-Young tube, a solution of trityl chloride (2 equiv) in THF was added to a solution of $\text{Fe}_3\text{H}_3\text{L}$ (1, 1 equiv) in THF at ambient temperature. The tube was closed, inverted, and shaken. After 2 h, a ^1H NMR spectra was recorded, indicating the formation of Gomberg's dimer and dihydrogen.

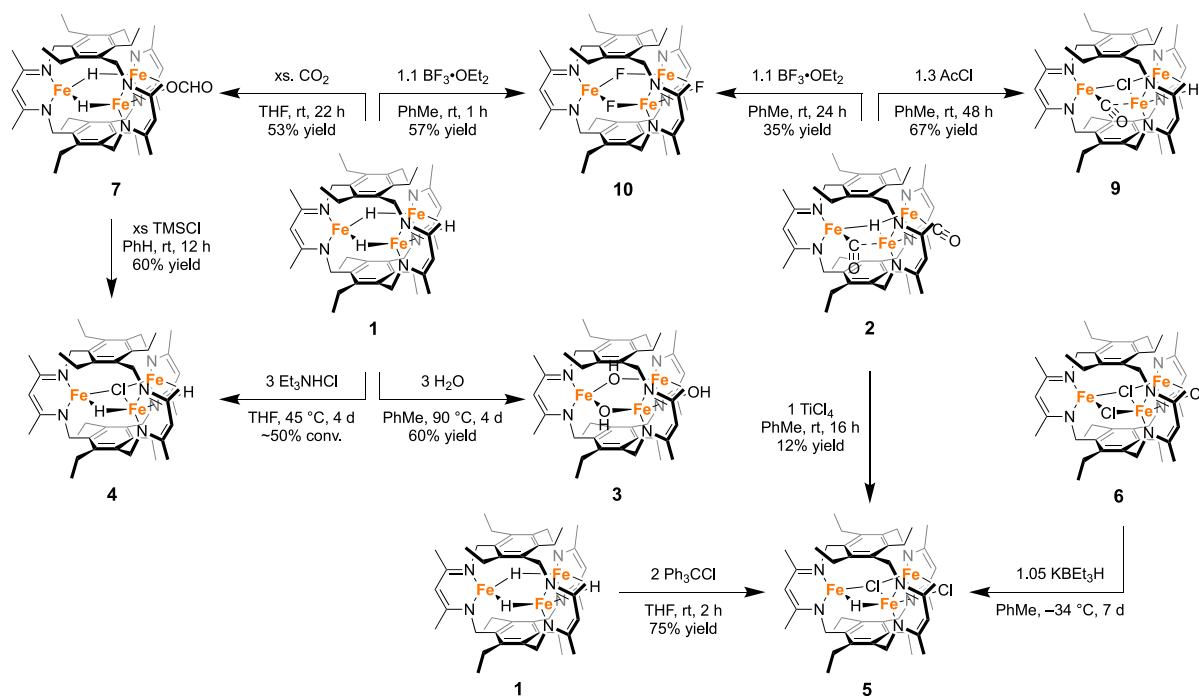
Detection of $\text{Fe}_3\text{HCl}_2\text{L}$ (5) from the Reaction of $\text{Fe}_3\text{Cl}_3\text{L}$ (6) with KHBET_3 . In a borosilicate jar with a glass stir bar, a solution of $\text{Fe}_3\text{Cl}_3\text{L}$ (6, 100 mg, 104 μmol) in toluene (60 mL) at -34 °C was charged with KHBET_3 (11.6 mg, 109 μmol), sealed with a Teflon cap, and stirred at -34 °C for 7 d. The reaction mixture was concentrated under reduced pressure. The residue was dissolved in benzene (40 mL), filtered through a plug of benzene-rinsed Celite, and the resulting solution was lyophilized. ^1H NMR analysis of the crude reaction mixture indicated a 26:23:2:1 mixture of $\text{Fe}_3\text{Cl}_3\text{L}$ (6)/ $\text{Fe}_3\text{HCl}_2\text{L}$ (5)/ $\text{Fe}_3\text{H}_2\text{CIL}$ (4)/ $\text{Fe}_3\text{H}_3\text{L}$ (1).

Detection of Intermediates in the Reaction of $(\text{FeCO})_2\text{Fe}(\mu_3\text{-H})\text{L}$ (2) with Organohalides. A J. Young NMR tube was charged with $(\text{FeCO})_2\text{Fe}(\mu_3\text{-H})\text{L}$ (2, 2.1 mg, 2.33 μmol), benzene- d_6 (400 μL), and then the organohalide (9.32 μmol). The tube was closed, inverted, and shaken. A ^1H NMR spectrum was recorded at 1, 12, 24, and 48 h.

Detection of CHDCl_2 in the Reaction of $(\text{FeCO})_2\text{Fe}(\mu_3\text{-H})\text{L}$ (2) with CHCl_3 in Toluene- d_8 . A J. Young NMR tube was charged with $(\text{FeCO})_2\text{Fe}(\mu_3\text{-H})\text{L}$ (2, 2.1 mg, 2.33 μmol) and toluene- d_8 (400 μL) and then CHCl_3 (0.75 μL , 9.32 μmol). The tube was closed, inverted, and shaken. The mixture slowly changed from light brown to a slight orange. After 4 d, the volatiles were then transferred to a second J. Young tube. A ^1H NMR spectrum was recorded, and CH_2Cl_2 was detected.

Detection of 1-Butene in the Reaction of $(\text{FeCO})_2\text{Fe}(\mu_3\text{-H})\text{L}$ (2) with (Cyclopropyl)methyl Chloride. A J. Young NMR tube was charged with $(\text{FeCO})_2\text{Fe}(\mu_3\text{-H})\text{L}$ (2, 2.1 mg, 2.33 μmol) and then THF- d_8 (400 μL) and (cyclopropyl)methyl chloride (0.85 μL , 9.32 μmol). The tube was closed, inverted, and shaken. The mixture slowly changed from light brown to a slight orange. At 1 h, a ^1H NMR spectrum was recorded, and 1-butene-4- d_1 was detected.

Scheme 1. Reactivity of 1 and 2



Reaction of $(\text{FeCO})_2\text{Fe}(\mu_3\text{-H})\text{L}$ (2) with $\text{BF}_3\cdot\text{OEt}_2$. A jar was charged with $(\text{FeCO})_2\text{Fe}(\mu_3\text{-H})\text{L}$ (2, 80.0 mg, 87.7 μmol), a Teflon-coated stir bars, and toluene (58 mL), followed by $\text{BF}_3\cdot\text{OEt}_2$ (10.8 μL , 87.7 μmol). The jar was then sealed with a Teflon-lined cap and stirred at 50 $^\circ\text{C}$. The dark green-yellow solution progressively changed to a dark yellow as it stirred for 24 h. The reaction mixture was then filtered through a plug of Celite, washed with toluene (2 mL), and then concentrated under reduced pressure. The crude solid was recrystallized from boiling benzene affording $\text{Fe}_3\text{F}_3\text{L}$ (10, 28.0 mg, 35% yield) as a yellow crystalline solid. The Celite plug was washed with THF (10 mL), and the filtrate was concentrated under reduced pressure to afford a gray solid (11.0 mg).

Detection of the Boron and Fluorine Byproducts in the Reaction of $(\text{FeCO})_2\text{Fe}(\mu_3\text{-H})\text{L}$ (2) with $\text{BF}_3\cdot\text{OEt}_2$. A J. Young NMR tube was charged with $(\text{FeCO})_2\text{Fe}(\mu_3\text{-H})\text{L}$ (2, 2.1 mg, 2.33 μmol) and benzene- d_6 (400 μL) and $\text{BF}_3\cdot\text{OEt}_2$ (1.2 μL , 9.32 μmol) at ambient temperature. The tube was closed, inverted, and shaken. The mixture changed from light brown to yellow within an hour. ^1H , ^{11}B , and ^{19}F NMR spectra were recorded in toluene- d_8 . The ^1H NMR indicates that the major paramagnetic species is $\text{Fe}_3\text{F}_3\text{L}$ (10). The ^{11}B and ^{19}F NMR exhibits peaks that our suggestive of polymerization.

Reaction of $(\text{FeCO})_2\text{Fe}(\mu_3\text{-H})\text{L}$ (2) with BCl_3 . A scintillation vial was charged with $(\text{FeCO})_2\text{Fe}(\mu_3\text{-H})\text{L}$ (2, 12.0 mg, 13.1 μmol), a Teflon-coated stir bar, and toluene (12 mL). The suspension was cooled to -35 $^\circ\text{C}$, and a solution of BCl_3 in *n*-hexane (1.0 M, 13.1 μL , 13.1 μmol) was added to the mixture. The vial was sealed with a Teflon-lined cap and stirred at -35 $^\circ\text{C}$. After 1 h, the mixture was warmed and stirred at ambient temperature. After 17 h, the dark amber solution was concentrated and a ^1H NMR spectrum was recorded in toluene- d_8 indicating that the primary product was $(\text{FeCO})\text{-Fe}_2\text{HCIL}$ (9).

Reaction of $(\text{FeCO})_2\text{Fe}(\mu_3\text{-H})\text{L}$ (2) with TiCl_4 . A scintillation vial was charged with $(\text{FeCO})_2\text{Fe}(\mu_3\text{-H})\text{L}$ (2, 12.0 mg, 13.1 μmol), a Teflon-coated stir bar, toluene (6.7 mL), and

then a solution of TiCl_4 in toluene (13.1 mM, 1.00 mL, 13.1 μmol). The vial was sealed with a Teflon-lined cap and stirred at ambient temperature. After 24 h, the dark orange-red solution was concentrated and a ^1H NMR spectrum was recorded in toluene- d_8 indicating that the primary product was $\text{Fe}_3\text{HCl}_2\text{L}$ (5).

Reaction of $(\text{FeCO})_2\text{Fe}(\mu_3\text{-H})\text{L}$ (2) with Cp_2TiCl_2 . A scintillation vial was charged with $(\text{FeCO})_2\text{Fe}(\mu_3\text{-H})\text{L}$ (2, 12.0 mg, 13.1 μmol), a glass-coated stir bar, toluene (12 mL), and then Cp_2TiCl_2 (3.3 mg, 13.1 μmol). The vial was sealed with a polyethylene-lined cap and stirred at ambient temperature. After 24 h, the orange-red solution was concentrated and a ^1H NMR spectrum was recorded in benzene- d_6 indicating that the primary product was $\text{Fe}_3\text{HCl}_2\text{L}$ (5).

Heating and Photolysis of $\text{Fe}_3\text{HCl}_2\text{L}$ (4), $\text{Fe}_3\text{HCl}_2\text{L}$ (5), $\text{Fe}_3\text{H}_2(\text{O}_2\text{CH})\text{L}$ (7), and $\text{Fe}_3\text{H}(\text{O}_2\text{CH})_2\text{L}$ (8). A J. Young NMR tube was charged with $\text{Fe}_3\text{H}_3\text{L}$ (1, 2.0 mg, 2.33 μmol) and benzene- d_6 (400 μL) at ambient temperature. The tube was closed, inverted, and shaken. The NMR tube was heated to 80 $^\circ\text{C}$ for 14 h and then a ^1H NMR spectrum was recorded. Then, the NMR tube was cooled to 10 $^\circ\text{C}$ in a water bath. This temperature was maintained while the reaction was photolyzed using a halogen lamp for 8 h. The spectra indicate no or limited reactivity upon heating and photolysis.

Crystallographic Procedure. A specimen of $\text{C}_{59}\text{H}_{82}\text{Fe}_3\text{N}_6\text{O}_3$, approximate dimensions of 0.068 mm \times 0.089 mm \times 0.126 mm, were used for the X-ray crystallographic analysis. The X-ray intensity data were measured ($\lambda = 0.71073$ \AA) using a Bruker Apex II single crystal diffractometer.

The integration of the data using a monoclinic unit cell yielded a total of 46287 reflections to a maximum θ angle of 27.50 $^\circ$ (0.77 \AA resolution), of which 12819 were independent (average redundancy 3.611, completeness = 98.7%, $R_{\text{int}} = 7.43\%$, $R_{\text{sig}} = 8.08\%$) and 10985 (85.69%) were greater than $2\sigma(F^2)$. The final cell constants of $a = 11.8048(10)$ \AA , $b = 11.7910(10)$ \AA , $c = 19.3233(16)$ \AA , $\beta = 90.585(2)^\circ$, volume = 2689.5(4) \AA^3 , are based upon the refinement of the XYZ-

centroids of reflections above 20 $\sigma(1)$. The calculated minimum and maximum transmission coefficients (based on crystal size) are 0.9010 and 0.9450.

The structure was solved and refined using the Bruker SHELXTL Software Package, using the space group P1n1, with $Z = 2$ for the formula unit, $C_{59}H_{82}Fe_3N_6O_3$. The final anisotropic full-matrix least-squares refinement on F^2 with 657 variables converged at $R1 = 7.76\%$, for the observed data and $wR2 = 19.70\%$ for all data. The goodness-of-fit was 1.044. The largest peak in the final difference electron density synthesis was $1.531 \text{ e}^-/\text{\AA}^3$ and the largest hole was $-0.984 \text{ e}^-/\text{\AA}^3$ with an RMS deviation of $0.114 \text{ e}^-/\text{\AA}^3$. On the basis of the final model, the calculated density was 1.347 g/cm^3 and $F(000)$, 1160 e^- .

RESULTS AND DISCUSSION

Given the prior hydridic reactivity of Fe_3H_3L (**1**),³⁹ we sought to investigate its reactivity with Brønsted acids. Reaction of **1** with 3 equiv of H_2O in PhMe at 90 °C for 3.5 d resulted in a color change from red to an amber orange (broad absorption with λ_{max} (nm) = 269, 332, 374, 384, 392, Figure S3) corresponding to the tri(μ -hydroxide) complex in near-quantitative spectroscopic yield and moderate crystalline yield (Scheme 1, 60% yield). This formulation of **3** is supported by single-crystal X-ray diffraction, combustion analysis, HR-ESI-MS(+), Mössbauer spectroscopy, and 1H NMR spectroscopy. The latter illustrates 5 peaks between 80.8 and -26.8 ppm as expected for a D_{3h} symmetric species in solution and on the method time scale (Figure S1). The bridging hydroxides were not observed in the 1H NMR spectrum, as one might expect given proximity to the paramagnetic Fe centers, but an O–H stretching vibration at 3642 cm^{-1} was observed in the IR spectrum (Figure S2). The solid-state structures of **3** evidence these bridging hydroxide ligands within a hexagonal planar $[Fe_3(X)_3]^{3+}$ core typical of other complexes supported by L^{3-} (Figure S4). The 80 K Mössbauer spectrum displays a single doublet (Table S1, Figure S6, $\delta = 0.94 \text{ mms}^{-1}$, $\Delta E_Q = 2.99 \text{ mms}^{-1}$) indicating three equivalent high-spin Fe^{II} centers. The slow reactivity of **1** with water is consistent with the previously observed substrate selectivity of M_3H_3L complexes [where $M = Fe^{II}, Co^{II}, Zn^{II}$ and L^{3-} is a tris(β -diketiminato) cyclophane].^{39,42} Investigations into the origin of this selectivity suggest the primary contributor to reaction rates is the steric crowding around the hydride pocket.⁴³

Furthermore, **1** reacts with 3 equiv of $[Et_3NH][Cl]$ in THF at 45 °C over 4 d resulting in a color change from red to yellow. Analysis of the reaction mixture by 1H NMR spectroscopy indicated a 50% conversion to Fe_3H_2CIL (**4**) (*vide infra*) without evidence of additional products by 1H NMR analysis (Scheme 1, Figure S17). Unfortunately, heating longer at this temperature to accomplish complete conversion resulted in the production of Fe_3HCl_2L (**5**) and Fe_3Cl_3L (**6**) as well as the production of significant insoluble material (*vide infra*). Optimization of this route to exclusively produce Fe_3H_2CIL (**4**) was unproductive; therefore, we pursued alternative methods to access **4** in higher purity and to confirm its structural assignment.

As previously reported, a 6:1 mixture of $Fe_3H_2(O_2CH)L/Fe_3H(O_2CH)_2L$ (**7:8**) could be produced through the reaction of **1** with CO_2 (Figure S18).³⁹ A solution of this mixture in benzene was treated with Me_3SiCl without stirring for 2 d, producing reddish-orange needles constituting a 6:1 mixture of

Fe_3H_2CIL (**4**)/ Fe_3HCl_2L (**5**), respectively. On rare occasions, **4** could be selectively recrystallized from **5**. The 1H NMR spectrum of **4** exhibits C_{2v} symmetry in solution with peaks between 134.1 and -54.2 ppm (Figure S7). Attempts to obtain single crystals sufficient for structural characterization of **4** have been unsuccessful thus far, and crystals yet obtained have been twinned with a cocrystallized impurity. Crystal packing of complexes supported by L^{3-} appear dominated by the ligand, which can lead to cocrystallization of multiple compounds in a single crystal, twinning, and poor crystal quality. As an example, a portion of the trihydride's (**1**) crystal structure has $\sim 3\%$ occupancy of Fe atoms with η_6 -binding.³⁹ Ultimately, the reactivity profile of complex **4** supports the assignment as the di(μ -hydride)(μ -chloride) complex (*vide infra*).

Given the above dehydrochlorination reactivity, is a hydride or an iron initially protonated? Iron hydride complexes undergo dehydrochlorination upon treatment with hydrochloric acid.⁴⁴ This typically proceeds through protonation of iron (i.e., oxidative addition) followed by reductive elimination of H_2 .^{45,46} As an alternative to iron protonation, hydride protonation remains plausible, despite a dearth of explicit examples in the literature. This hydride protonation mechanism was previously implicated in the FeMoco catalytic cycle, though later studies indicated a reductive elimination mechanism predominates.¹⁸ Holland et al. reported the reactivity between $[(\beta\text{-diketiminato})Fe(\mu\text{-H})]_2$ complexes and weak Brønsted acids.³⁰ Using literature values in DMSO, they suggested β -diketiminato iron hydrides can be protonated with acids of pK_a values up to 32 (or possibly higher). Again, hydride protonation was implied but not explicitly evidenced. Unlike Holland's examples, the present complexes are unambiguously multi-iron clusters. Upon hydride protonation, the cationic charge should be better supported between all metal centers, though this particular pathway still remains unclear.

To complement the hydridic reactivity studies, we investigated reactivity of **1** in net hydrogen-atom transfer reactions with organochloride substrates. If successful, we anticipated that such an approach would also provide a synthetically practical method for accessing **4** or **5** in high purity. To initiate our reactivity study, we settled on standard conditions consisting of 4 equiv of the organochloride substrate in benzene- d_6 at rt (Figure 2).⁴⁷ Trihydride **1** was treated with CCl_4 , $CHCl_3$, and CH_2Cl_2 with more oxidized substrates reacting faster, whereas monochlorides $BnCl$, $t\text{-BuCl}$, and (cyclopropyl)methyl chloride were unreactive (Figures S19–S24). The *in situ* 1H NMR spectrum of **1** with 4 equiv of $CHCl_3$ in benzene- d_6 produces **4**, followed by **5**, and finally **6** (Figures 2, S20). The volatiles of this reaction indicate the formation of CH_2Cl_2 (Figure S26).

This reactivity trend generally, but not fully, corresponds to the organochloride's BDEs. As an example of the discrepancy, the BDE for $BnCl$ and $CHCl_3$ are 71.7 and 82.8 kcal/mol, respectively, yet the latter readily reacts and the former does not.^{48–50} Reversible alkyl chloride coordination may proceed rate-limiting electron-transfer, and then, dissociation and diffusion of the alkyl radical. If this is the predominate mechanism among all substrates, $CHCl_3$ and $t\text{-BuCl}$ would react analogously given their comparable reduction potentials ($-2.58 \text{ V vs Ag/Ag}^+$ and -2.60 V vs SCE , respectively).^{51,52} Additionally, CH_2Cl_2 and $BnCl$ would have similar reactivity given their reduction potentials (-1.7 V vs SCE and -1.8 V vs SCE , respectively).⁵³ Since $t\text{-BuCl}$ and $BnCl$ are unreactive,

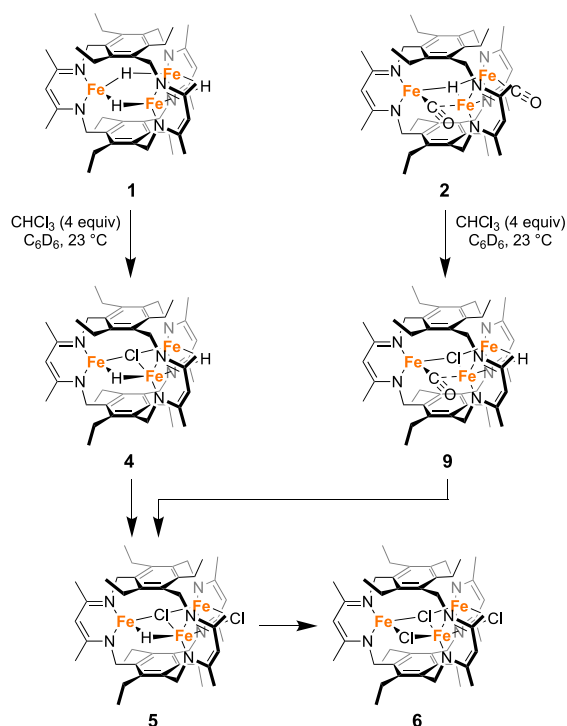


Figure 2. Convergent cascade reactions of **1** or **2** with chloroform to ultimately afford **6**.

ligand sterics may again limit access to the iron centers precluding the electron transfer event.

If the reaction is radical in nature, one possible mechanism is diffusion of the carbon-centered radical from the proposed product complex prior to hydrogen-atom abstraction. Then, the downstream reactivity of the freely diffusing radical would afford distinct products as compared to the possible concerted mechanisms (e.g., S_N2). A proposed mechanism of the reaction between **1** and chloroform is described in Figure 3A. Analogous to the proposed initial CO_2 coordination for reaction of **1** with CO_2 , coordination of the organochloride substrate to the trimetallic complex occurs first. In contrast to CO_2 migratory insertion, however, substrate coordination is followed by homolytic bond cleavage of the C–Cl bond to give a dichloromethyl radical and the mixed valent $Fe^{III}Fe^{II}_2$ cluster (**11**). Hydrogen-atom transfer from this cluster to the dichloromethyl radical provides complex **4** and dichloromethane. This mechanism may undergo two additional chlorine-atom abstractions/hydrogen-atom transfers to ultimately afford Fe_3Cl_3L (**6**).

To provide support for the radical pathway, we performed a crossover experiment between **1-D** and 20 equiv of chloroform (Figure 3B). The volatiles of this reaction contained a 2:1 ratio of dichloromethane- d_1 and dichloromethane, respectively (Figure S27), consistent with a radical mechanism. Initial chlorine-atom abstraction from chloroform by **1-D** (Figure 3C, Step A) followed by deuterium-atom abstraction by the dichloromethyl radical from the mixed valent cluster results in **4-D** and the formation of $CHDCl_2$ (Figure 3C, Step B). Alternatively, a propagation step may occur where the dichloromethyl radical reacts with another molecule of chloroform producing the more stable trichloromethyl radical (Figure 3C, Step C).^{48,54,55} Termination occurs upon deuterium-atom abstraction from the mixed-valent complex to afford **4-D** and chloroform- d_1 (Figure 3C, Step D).

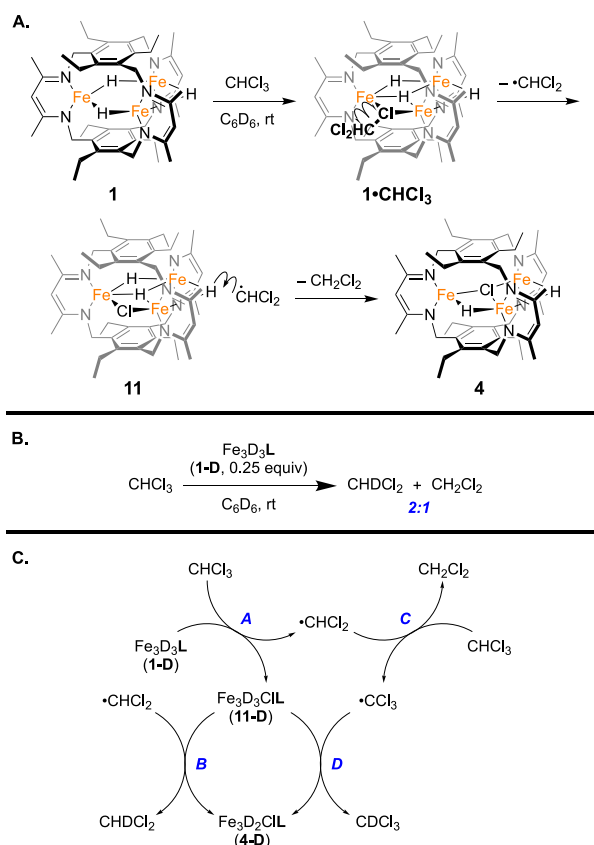
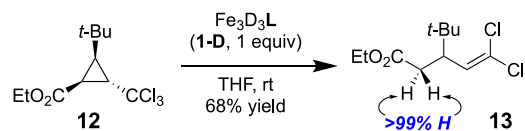


Figure 3. (A) Proposed mechanism for the formation of **4** from the reaction of **1** and chloroform. (B) Formation of $CHDCl_2$ and CH_2Cl_2 when **1-D** is reacted with $CHCl_3$. (C) Radical propagation mechanism for the formation of $CHDCl_2$ and CH_2Cl_2 .

Substrates bearing cyclopropyl rings have strong precedent as probes for radical reactions.^{56,57} Thus, we reacted **1-D** with 1 equiv of trichloride **12** in THF at rt, which afforded dichloroalkene **13** in 68% yield and with >99% H incorporation at the α -position (Scheme 2, Figure S28). This

Scheme 2. Cyclopropane Ring-Opening of **12** When Reacted with **13** Indicating a Radical Mechanism



outcome supports an initial chlorine-atom abstraction from the **12** by the trimetallic complex, followed by a radical ring-opening of the cyclopropane, and then abstraction of a hydrogen-atom from the solvent to afford dichloroalkene **13**.^{58,59}

Alternative mechanistic hypotheses were considered. A bimolecular nucleophilic substitution (S_N2) mechanism is inconsistent with the observed reactivity pattern since many electrophiles, like dichloromethane, are more reactive with **1** than methyl iodide (Figures S21 vs S25). A σ -bond metathesis may be feasible but should be sterically demanding within this ligand system. Due to these steric constraints, other unconventional mechanistic pathways were also considered. Halogenophilic bimolecular nucleophilic substitution (S_N2Hal) (i.e., hydride attack at the halogen) is generally consistent with the

observed substrate reactivity pattern but would be unusual.⁶⁰ Additionally, this mechanistic pathway produces HCl, and the *in situ* NMR spectra of these reactions do not evidence the free ligand (H₃L), an expected byproduct in the presence of strong acids.

Given the reaction between complex **1** and organochlorides produces complex **4**, which arises from H atom transfer/abstraction by the freely diffusing radical, we speculated that an intermediate to **4** or an alternative product could be accessed if the rate of radical termination sufficiently exceeded hydrogen-atom transfer. Triphenylmethane has a weak C–H BDE, its radical is more stable than those of other chlorinated alkanes, and the trityl radical undergoes facile dimerization to Gomberg's dimer as a means of termination, usually instead of hydrogen-atom abstraction. Therefore, **1** was reacted with trityl chloride (2 equiv) in THF at rt (Scheme 1). Satisfyingly, the reaction produced cluster **5** without the formation of cluster **4** by ¹H NMR spectroscopy (Figure S29). The product mixture was triturated in pentane and filtered to afford sufficiently pure material of complex **5** for downstream chemistry, though impurities were still observed by ¹H NMR analysis. As expected, the *in situ* ¹H NMR spectrum exhibited Gomberg's dimer and dihydrogen (Figure S30). Given these results, intermediate **11** likely reductively eliminates H₂ in the absence of a radical species competent for hydrogen-atom abstraction from the cluster (Figure 4). The resulting Kubas

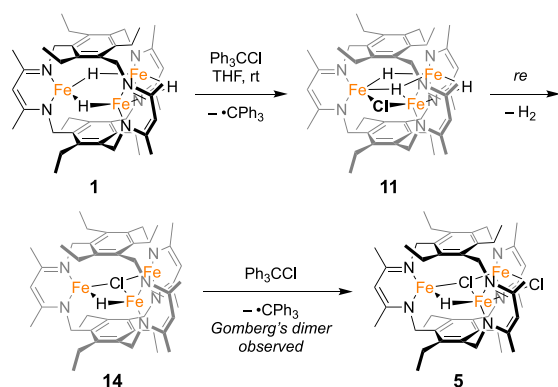


Figure 4. Proposed mechanism for the formation of **5** from the reaction of **1** and trityl chloride.

complex or compound **14** is poised to react with a second equivalent of trityl chloride to afford cluster **5**. Alternative synthetic methods support this structural assignment. Treating Fe₃Cl₃L (**6**) with KBHET₃ initially produced **5**, though this reaction was unselective and prolonged reaction times result in overreduction (Scheme 1, Figure S31).

Iron-mediated hydrodehalogenation of organic halides has been robustly studied.⁶¹ Specific to iron hydrides, complexes within a strong field react with CHCl₃ and CH₂Cl₂ resulting in hydride-for-chloride exchange products.^{62–67} Mechanistically, iron hydride complexes within these ligand fields engage in radical reactivity. As an example, mixtures of CpFe(CO)(PPh₃)H in CH₂Cl₂ afford CpFe(CO)(PPh₃)Cl when treated with Gomberg's dimer.⁶⁸ Complex **1** displays similar reactivity to these other iron hydride systems when treated with organochlorides. Notably, the synthesis of **5** from **1** and trityl chloride is a rare selective hydride-for-chloride substitution in an iron cluster, resulting in a mixed-substitution complex.⁶⁹ These mixed hydride/chloride complexes may serve as

strategic precursors in the synthesis of designed iron hydride clusters decorated with *N*- and *S*-ligands, aimed at modeling the reactivity of biologically relevant nitrogenase cofactors, such as FeMoco.

We hypothesized that (FeCO)₂Fe(μ₃-H)L (**2**) with formal triiron(I/I/II) valences might arrest after chloride-atom abstraction with loss of one or more CO donors. Alternatively, we speculated that an oxidative addition pathway may be available, especially if the hydride remained within the cyclophane complex and inaccessible during the course of the reaction.^{70,71} This pathway was particularly desired as it might install a C₁-ligand, which would be useful in accessing biologically relevant model systems.²⁹ Thus, in an analogous set of experiments, (FeCO)₂Fe(μ₃-H)L (**2**) was reacted with a larger suite of organochlorides and reactions monitored by ¹H NMR spectroscopy (Figures S32–S40). As with **1**, reactions are faster for more oxidized organochlorides (e.g., CCl₄ > CHCl₃ > CH₂Cl₂), and similarly, reaction of **2** with CHCl₃ in toluene-*d*₈ produces CH₂Cl₂ from ¹H NMR spectroscopy of the reaction volatiles (Figure S41). *n*-Butyl chloride was unreactive with **2**, whereas *t*-butyl chloride slowly reacts at rt. Dichloroethane had a similar rate as *t*-butyl chloride, and monochlorides with activating groups (e.g., benzyl chloride and (cyclopropyl)methyl chloride) were significantly faster. When the reaction with (cyclopropyl)methyl chloride was conducted in THF-*d*₈, the *in situ* ¹H NMR spectrum evidenced 1-butene-*d*₁ (Figure S42) indicating chlorine-abstraction, radical ring-opening of the cyclopropane, and deuterium-abstraction from the solvent. Chlorobenzene, unlike most of the alkyl chlorides, was unreactive. Surprisingly, when bromotrichloromethane was used (Figure S43), the complexes observed by ¹H NMR spectroscopy were the chlorinated complexes obtained with organochlorides (e.g., **9**, **5**, and **6**, *vide infra*). Homolytic cleavage of bromotrichloromethane's C–Br bond is more favorable than cleavage of the C–Cl bond,^{72,73} which may suggest a requisite coordination of the halide with the iron centers prior to homolysis. Again, selectivity may derive from the ligand's steric discrimination between chloride and bromide, though this selectivity may simply derive from greater strength of the Fe–Cl vs Fe–Br bond.

A previously unknown compound, (FeCO)Fe₂HClIL (**9**), was consistently observed as the initial intermediate upon reacting **2** with organochlorides. To confirm this assignment, we sought to independently synthesize this species. Among the organochlorides assessed, acetyl chloride was ultimately superior. A solution of triiron cluster **2** in toluene at ambient temperature was charged 4 times with acetyl chloride resulting in a total of 1.3 equiv over 9 d. The ¹H NMR spectrum indicates a complex mixture with (FeCO)Fe₂HClIL (**9**) as the major product, full consumption of the starting material, and minimal formation of dichloride **5** (Figure S13). The species is C_s symmetric on the instrument time scale. Although stable in the solid state for extended periods, attempts to crystallize **9** were unsuccessful, as the compound decomposed in solution over long periods of time, with Fe₃(OH)₃L (**3**) as the commonly observed decomposition product. This inability to purify **9** precluded characterization by elemental analysis, but, fortunately, we were able to obtain satisfactory electrospray ionization mass spectra (Figure S16). The two most abundant observed ions were at *m/z* = 920.3060, assigned to the protonated ion [9+H]⁺, and *m/z* = 904.3113, assigned to the [Fe₃O₃L+H]⁺, which forms in the course of the MS

experiment. The observed mass shifts to $m/z = 921.2971$ and $m/z = 921.2959$ when **9** is synthesized from the D-labeled or ^{13}C -labeled isotopologue of **2**, respectively, strongly supporting our assignment of **9**. The strong IR absorption of **2** at 1846 cm^{-1} undergoes a slight hypsochromic shift to 1850 cm^{-1} in **9** and decreases in intensity by $\sim 1/2$ as anticipated for one-electron oxidation of the cluster and retention of a semi-bridging CO donor (Figure S14). In **2**, only one IR absorption is observed for the CO stretching modes, presumable due to weak coupling between each of the two C–O stretching modes; decrease in intensity then would be consistent with loss of a single CO ligand. This absorption in the spectrum of **9** shifts to 1807 cm^{-1} for the ^{13}C -labeled complex ($9\text{-}^{13}\text{C}$) (theoretical/observed $\Delta\nu(^{12}\text{C}\text{O}-^{13}\text{C}\text{O}) = 41/43\text{ cm}^{-1}$) (Figure S15). These results agree with arresting the reactivity at chloride abstraction with loss of one carbonyl ligand to afford **9**, which may be repeated with a second equivalent of organochloride to afford **5** (Figure 5).

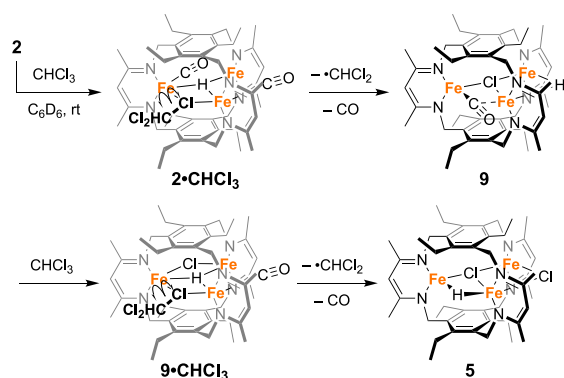


Figure 5. Proposed mechanism for the formation of **9** and **5** from the reaction of **2** and chloroform.

We previously reported the reaction of **1** with $\text{BF}_3\cdot\text{OEt}_2$ in toluene to afford $\text{Fe}_3(\mu\text{-F})_3\text{L}$ (**10**, Scheme 1).⁴¹ Given that metal carbonyls are activated by Lewis acids, we speculated that complex **2** would display divergent reactivity from **1** when treated with $\text{BF}_3\cdot\text{OEt}_2$.^{74–76} Specifically, metal carbonyl hydrides undergo formal hydrogen migration to afford formyl complexes when treated with Lewis acids.⁷⁷ Additionally, silyl Lewis acids have been shown to access carbyne and carbide species from low-valent iron complexes.^{78–80} To our surprise, reactions of **2** with $\text{BF}_3\cdot\text{OEt}_2$ in toluene at rt converge to **10** over 2 h. Ultimately, a byproduct precipitates as red fibers leaving a bright yellow solution. Once the byproduct precipitates, the solution exhibits a ^1H NMR (Figure S45) and IR spectrum of predominantly complex **10**. Upon filtration, the fibrous material is insoluble in hydrocarbons and THF and exhibits an IR absorption at 1870 cm^{-1} (Figure S46). Since **10** is 2 electrons more oxidized than complex **2**, we propose that this byproduct is a boron cluster or polymer containing one or more semibridging carbonyls. Examples of carbonyl-containing fluoroboranes are difficult to find in the literature; however, carbonyl-containing diboron clusters have been reported by Braunschweig. Clusters with a bridging carbonyl have $\nu(\text{C}=\text{O})$ IR stretches between $\nu = 1690\text{--}1706\text{ cm}^{-1}$,^{81–83} while a lone diboron cluster has an IR stretch at 1926 cm^{-1} corresponding to a semibridging carbonyl.^{84,85} Substituting BCl_3 for $\text{BF}_3\cdot\text{OEt}_2$ generates a mixture similar to

when organochlorides are used with **9**, **5**, and **6** all being observed (Figure S48).

Attempting to activate the iron carbonyl in a similar fashion to the boron-Lewis acids, we reacted **2** with 1 equiv of Cp_2TiCl_2 or TiCl_4 (Scheme 1, Figures S49, S51). Surprisingly, both cases produced **5** as the major product. Addition of either titanium electrophile at rt changes the solution from dark yellow-green to red. In the case of TiCl_4 , the product was crystallized from a $90\text{ }^\circ\text{C}$ toluene solution to afford large red crystals (broad absorption with λ_{max} (nm) = 327, 400, 420, 551, Figure S11) consisting of a 14:1 mixture of **5**:**6**. Cluster **5** was further characterized by HR-ESI-MS(+) (Figure S12) and ^1H NMR spectroscopy (Figure S9). The latter method supports an assignment of a C_{2v} symmetric compound with 10 resonances between 170.1 and -53.9 ppm. Dechlorination of titanium complexes has been reported with FeCl_3 , via chloride exchange or transmetalation, though not with low-valent molecular iron species.^{86,87}

With all four hydride/chloride complexes **1** and **4–6** in hand, their properties could be compared. The $\text{C}=\text{N}$ stretching vibrations of chloride complexes **4**, **5**, and **6** display bathochromic shifts compared to trihydride **1** (1517 , 1519 , 1518 , vs 1526 cm^{-1} , respectively). The solution magnetic susceptibility of **4**, **5**, and **6** are 6.2 , 7.2 , and $7.2\ \mu_{\text{B}}$, respectively. These values are consistent with other triiron(II) complexes supported by L^{3-} ($6.2\text{--}7.5\ \mu_{\text{B}}$). Furthermore, iron hydride complexes **4** and **5** were thermally stable under argon at $80\text{ }^\circ\text{C}$ in benzene- d_6 for 14 h, and stable to irradiation using a broad-spectrum halogen lamp at $10\text{ }^\circ\text{C}$ for 8 h.⁸⁸ This reactivity is similar to **1**, which required CO and not thermal or photolytic conditions to undergo reductive elimination.

CONCLUSION

This study was initiated to explore the reactivity profile of bridging hydrides within high-spin iron clusters of different oxidation states and coordination environments. Regarding this effort, we investigated the reactivity of triiron hydride clusters $\text{Fe}_3\text{H}_3\text{L}$ (**1**) and $(\text{FeCO})_2\text{Fe}(\mu_3\text{-H})\text{L}$ (**2**). Complex **1** was treated with H_2O and $[\text{Et}_3\text{NH}][\text{Cl}]$ exhibiting muted hydride-like character analogous to its reactivity with CO_2 . Both **1** and **2** undergo radical reactivity when treated with organochlorides such as CHCl_3 . These combined studies produced synthetic methods to access mixed-hydride/chloride clusters $\text{Fe}_3\text{H}_2\text{ClL}$ (**4**), $\text{Fe}_3\text{HCl}_2\text{L}$ (**5**), and $\text{Fe}^{\text{I}}\text{Fe}^{\text{II}}$ cluster $(\text{FeCO})\text{Fe}_2\text{HCl}_2\text{L}$ (**9**). Further studies on the reactivity of triiron hydride clusters is ongoing.

ASSOCIATED CONTENT

Supporting Information

The Supporting Information is available free of charge at <https://pubs.acs.org/doi/10.1021/acs.inorgchem.5c00071>.

^1H NMR; IR; ESI(+)/HRMS; Mössbauer data (PDF)

Accession Codes

Deposition number 2391224 contains the supplementary crystallographic data for this paper. These data can be obtained free of charge via the joint Cambridge Crystallographic Data Centre (CCDC) and Fachinformationszentrum Karlsruhe Access Structures service.

AUTHOR INFORMATION

Corresponding Author

Leslie J. Murray – Center for Catalysis and Florida Center for Heterocyclic Chemistry, Department of Chemistry, University of Florida, Gainesville, Florida 32611, United States; orcid.org/0000-0002-1568-958X; Email: murray@chem.ufl.edu

Authors

Brian J. Knight – Center for Catalysis and Florida Center for Heterocyclic Chemistry, Department of Chemistry, University of Florida, Gainesville, Florida 32611, United States

Kevin J. Anderton – Center for Catalysis and Florida Center for Heterocyclic Chemistry, Department of Chemistry, University of Florida, Gainesville, Florida 32611, United States

Juan F. Torres – Center for Catalysis and Florida Center for Heterocyclic Chemistry, Department of Chemistry, University of Florida, Gainesville, Florida 32611, United States

Vincent J. Catalano – Department of Chemistry, University of Nevada, Reno, Nevada 89557, United States; orcid.org/0000-0003-2151-2892

Ricardo Garcia-Serres – CNRS, CEA, BIG, LCBM (UMR 5249), Université Grenoble Alpes, Grenoble F-38054, France; orcid.org/0000-0001-5203-0568

Complete contact information is available at:

<https://pubs.acs.org/10.1021/acs.inorgchem.5c00071>

Author Contributions

The manuscript was written through contributions of all authors. All authors have given approval to the final version of the manuscript.

Notes

The authors declare no competing financial interest.

ACKNOWLEDGMENTS

Support for L.J.M. is provided by the National Institutes of Health (NIH), through grant no. R01-GM123241. The content is solely the responsibility of the authors and does not necessarily represent the official views of the National Institutes of Health. R.G.S. thanks Labex Arcane, CBH-EUR-GS (ANR-17-EURE-0003) for financial support.

REFERENCES

- (1) Mueller, M. W.; Blackledge, J. P.; Libowitz, G. G. *Metal Hydrides*; Academic Press Inc.: New York, 1968.
- (2) Peruzzini, M.; Poli, R. *Recent Advances in Hydride Chemistry*; Elsevier: New York, 2001.
- (3) McGrady, G. S.; Guilera, G. The Multifarious World of Transition Metal Hydrides. *Chem. Soc. Rev.* **2003**, *32*, 383–392.
- (4) Darenbourg, M. Y.; Ash, C. Anionic Transition Metal Hydrides. *Adv. Organomet. Chem.* **1987**, *27*, 1–50.
- (5) Hu, Y.; Shaw, A. P.; Estes, D. P.; Norton, J. R. Transition-Metal Hydride Radical Cations. *Chem. Rev.* **2016**, *116* (15), 8427–8462.
- (6) Overett, M. J.; Hill, O. R.; Moss, J. R. Organometallic Chemistry and Surface Science: Mechanistic Models for the Fischer–Tropsch Synthesis. *Coord. Chem. Rev.* **2000**, *206–207*, 581–605.
- (7) Franke, R.; Selent, D.; Börner, A. Applied Hydroformylation. *Chem. Rev.* **2012**, *112* (11), 5675–5732.
- (8) Christiansen, L. J.; Stoltze, P.; Aika, K.; Tamara, K.; Hansen, J. B.; Nielsen, P. E. H.; Dybkjaer, I.; Nielsen, A. *Ammonia: catalysis and Manufacture*; Springer: Berlin, 1995.
- (9) Klankermayer, J.; Wesselbaum, S.; Beydoun, K.; Leitner, W. Selective Catalytic Synthesis Using the Combination of Carbon

Dioxide and Hydrogen: Catalytic Chess at the Interface of Energy and Chemistry. *Angew. Chem., Int. Ed.* **2016**, *55* (26), 7296–7343.

(10) Qiao, J.; Liu, Y.; Hong, F.; Zhang, J. A Review of Catalysts for the Electroreduction of Carbon Dioxide to Produce Low-Carbon Fuels. *Chem. Soc. Rev.* **2014**, *43*, 631–675.

(11) Crossley, S. W. M.; Obradors, C.; Martinez, R. M.; Shenvi, R. A. Mn-, Fe-, and Co-Catalyzed Radical Hydrofunctionalizations of Olefins. *Chem. Rev.* **2016**, *116* (15), 8912–9000.

(12) Lo, J. C.; Kim, D.; Pan, C.-M.; Edwards, J. T.; Yabe, Y.; Gui, J.; Qin, T.; Gutiérrez, S.; Giacomoni, J.; Smith, M. W.; Holland, P. L.; Baran, P. S. Fe-Catalyzed C–C Bond Construction from Olefins via Radicals. *J. Am. Chem. Soc.* **2017**, *139* (6), 2484–2503.

(13) Nakazawa, H.; Itazaki, M. Fe–H Complexes in Catalysis. In *Iron Catalysis*, Plietke, B., ed.; Springer: Berlin, 2011, pp. 27–81.

(14) Honkala, K.; Hellman, A.; Remediakis, I. N.; Logadottir, A.; Carlsson, A.; Dahl, S.; Christensen, C. H.; Nørskov, J. K. Ammonia Synthesis from First-Principles Calculations. *Science* **2005**, *307* (5709), 555–558.

(15) Mager-Maury, C.; Bonnard, G.; Chizallet, C.; Sautet, P.; Raybaud, P. H₂-Induced Reconstruction of Supported Pt Clusters: Metal–Support Interaction versus Surface Hydride. *ChemCatchem* **2011**, *3* (1), 200–207.

(16) Schilter, D.; Camara, J. M.; Huynh, M. T.; Hammes-Schiffer, S.; Rauchfuss, T. B. Hydrogenase Enzymes and Their Synthetic Models: The Role of Metal Hydrides. *Chem. Rev.* **2016**, *116* (15), 8693–8749.

(17) Burgess, B. K.; Lowe, D. J. Mechanism of Molybdenum Nitrogenase. *Chem. Rev.* **1996**, *96* (7), 2983–3012.

(18) Hoffman, B. M.; Lukoyanov, D.; Yang, Z.-Y.; Dean, D. R.; Seefeldt, L. C. Mechanism of Nitrogen Fixation by Nitrogenase: The Next Stage. *Chem. Rev.* **2014**, *114* (8), 4041–4062.

(19) Adams, R. D.; Captain, B. Hydrogen Activation by Unsaturated Mixed-Metal Cluster Complexes: New Directions. *Angew. Chem., Int. Ed.* **2008**, *47* (2), 252–257.

(20) Besora, M.; Lledós, A.; Maseras, F. Protonation of Transition-Metal Hydrides: A Not so Simple Process. *Chem. Soc. Rev.* **2009**, *38*, 957–966.

(21) Araake, R.; Sakadani, K.; Tada, M.; Sakai, Y.; Ohki, Y. [Fe₆] and [Fe₆] Hydride Clusters Supported by Phosphines: Synthesis, Characterization, and Application in N₂ Reduction. *J. Am. Chem. Soc.* **2017**, *139* (15), 5596–5606.

(22) Wiedner, E. S.; Chambers, M. B.; Pitman, C. L.; Bullock, R. M.; Miller, A. J. M.; Appel, A. M. Thermodynamic Hydricity of Transition Metal Hydrides. *Chem. Rev.* **2016**, *116* (15), 8655–8692.

(23) Morris, R. H. Brønsted–Lowry Acid Strength of Metal Hydride and Dihydrogen Complexes. *Chem. Rev.* **2016**, *116* (15), 8588–8654.

(24) Poli, R. Open-Shell Organometallics as a Bridge between Werner-Type and Low-Valent Organometallic Complexes. The Effect of the Spin State on the Stability, Reactivity, and Structure. *Chem. Rev.* **1996**, *96* (6), 2135–2204.

(25) Schröder, D.; Shaik, S.; Schwarz, H. Two-State Reactivity as a New Concept in Organometallic Chemistry. *Acc. Chem. Res.* **2000**, *33* (3), 139–145.

(26) Harvey, J. N.; Poli, R.; Smith, K. M. Understanding the Reactivity of Transition Metal Complexes Involving Multiple Spin States. *Coord. Chem. Rev.* **2003**, *238–239*, 347–361.

(27) Poli, R.; Harvey, J. N. Spin Forbidden Chemical Reactions of Transition Metal Compounds. New Ideas and New Computational Challenges. *Chem. Soc. Rev.* **2003**, *32*, 1–8.

(28) Holland, P. L. Distinctive Reaction Pathways at Base Metals in High-Spin Organometallic Catalysts. *Acc. Chem. Res.* **2015**, *48* (6), 1696–1702.

(29) Čorić, I.; Holland, P. L. Insight into the Iron–Molybdenum Cofactor of Nitrogenase from Synthetic Iron Complexes with Sulfur, Carbon, and Hydride Ligands. *J. Am. Chem. Soc.* **2016**, *138* (23), 7200–7211.

(30) Yu, Y.; Sadique, A. R.; Smith, J. M.; Dugan, T. R.; Cowley, R. E.; Brennessel, W. W.; Flaschenriem, C. J.; Bill, E.; Cundari, T. R.; Holland, P. L. The Reactivity Patterns of Low-Coordinate Iron–Hydride Complexes. *J. Am. Chem. Soc.* **2008**, *130* (20), 6624–6638.

- (31) Gehring, H.; Metzinger, R.; Braun, B.; Herwig, C.; Harder, S.; Ray, K.; Limberg, C. An Iron(II) Hydride Complex of a Ligand with Two Adjacent β -Diketiminato Binding Sites and its Reactivity. *Dalton Trans.* **2016**, *45*, 2989–2996.
- (32) Hein, N. M.; Pick, F. S.; Fryzuk, M. D. Synthesis and Reactivity of a Low-Coordinate Iron(II) Hydride Complex: Applications in Catalytic Hydrodefluorination. *Inorg. Chem.* **2017**, *56* (23), 14513–14523.
- (33) Ott, J. C.; Blasius, C. K.; Wadepohl, H.; Gade, L. H. Synthesis, Characterization, and Reactivity of a High-Spin Iron(II) Hydrido Complex Supported by a PNP Pincer Ligand and Its Application as a Homogenous Catalyst for the Hydrogenation of Alkenes. *Inorg. Chem.* **2018**, *57* (6), 3183–3191.
- (34) Some iron hydride dimers lack a monomer/dimer equilibrium, see Hickey, A. K.; Greer, S. M.; Valdez-Moreira, J. A.; Lutz, S. A.; Pink, M.; DeGayner, J. A.; Harris, T. D.; Hill, S.; Telsler, J.; Smith, J. M. A Dimeric Hydride-Bridged Complex with Geometrically Distinct Iron Centers Giving Rise to an $S = 3$ Ground State. *J. Am. Chem. Soc.* **2019**, *141* (30), 11970–11975.
- (35) Ermert, D. M.; Murray, L. J. Insights into Small Molecule Activation by Multinuclear First-Row Transition Metal Cyclophanates. *Dalton Trans.* **2016**, *45*, 14499–14507.
- (36) Ferreira, R. B.; Cook, B. J.; Knight, B. J.; Catalano, V. J.; Garcia-Serres, R.; Murray, L. J. Catalytic Silylation of Dinitrogen by a Family of Triiron Complexes. *ACS Catal.* **2018**, *8* (8), 7208–7212.
- (37) Ferreira, R. B.; Murray, L. J. Cyclophanes as Platforms for Reactive Multimetallic Complexes. *Acc. Chem. Res.* **2019**, *52* (2), 447–455.
- (38) Eaton, M. C.; Catalano, V. J.; Shearer, J.; Murray, L. J. Dinitrogen Insertion and Cleavage by a Metal–Metal Bonded Tricobalt(I) Cluster. *J. Am. Chem. Soc.* **2021**, *143* (15), 5649–5653.
- (39) Lee, Y.; Anderton, K. J.; Sloane, F. T.; Ermert, D. M.; Abboud, K. A.; Garcia-Serres, R.; Murray, L. J. Reactivity of Hydride Bridges in High-Spin $[3M-3(\mu-H)]$ Clusters ($M = Fe^{II}, Co^{II}$). *J. Am. Chem. Soc.* **2015**, *137* (33), 10610–10617.
- (40) Hong, D. H.; Murray, J. L. Carbon Dioxide Insertion into Bridging Iron Hydrides: Kinetic and Mechanistic Studies. *Eur. J. Inorg. Chem.* **2019**, *15*, 2146–2153.
- (41) Anderton, K. J.; Knight, B. J.; Rheingold, A. L.; Abboud, K. A.; Garcia-Serres, R.; Murray, L. J. Reactivity of Hydride Bridges in a High-Spin $[Fe_3(\mu-H)_3]^{3+}$ Cluster: Reversible H_2/CO Exchange and Fe–H/B–F Bond Metathesis. *Chem. Sci.* **2017**, *8*, 4123–4129.
- (42) Ermert, D. M.; Ghiviriga, I.; Catalano, V. J.; Shearer, J.; Murray, L. J. An Air- and Water-Tolerant Zinc Hydride Cluster That Reacts Selectively with CO_2 . *Angew. Chem., Int. Ed.* **2015**, *54* (24), 7047–7050.
- (43) Hong, D. H.; Ferreira, R. B.; Catalano, V. J.; Garcia-Serres, R.; Shearer, J.; Murray, L. J. Access to Metal Centers and Fluxional Hydride Coordination Integral for CO_2 Insertion into $[Fe_3(\mu-H)_3]^{3+}$ Clusters. *Inorg. Chem.* **2021**, *60* (10), 7228–7239.
- (44) Song, L.-C.; Feng, L.; Lu, Y.; Yang, X.-Y. Synthesis, Structures, and Reactivity of $[NiFe]-H_2$ ase Mimics Containing One Square-Planar N_2S_2 Ligand Bridged between Their Ni/Fe Centers through One or Two S Atoms. *Organometallics* **2021**, *40* (4), 508–519.
- (45) Henderson, R. A. Mechanistic Studies on Iron Phosphine Complexes. Part 1. Protonation and Substitution of trans- $[FeH(X)(diphosphine)_2]$ ($X = Cl$ or Br , diphosphine = $Et_2PCH_2CH_2Pet_2$ or $Ph_2PCH_2CH_2PPh_2$). *J. Chem. Soc., Dalton Trans.* **1988**, 509–514.
- (46) Jenkins, H. A.; Loeb, S. J.; Dick, D. G.; Stephan, D. W. Dihydride Formation Versus H_2 -Elimination in the Protonation of the Heterobimetallic FePt Complex $(CO)_3Fe(\mu-H)(\mu-PCy_2)Pt(PEt_3)_2$. *Can. J. Chem.* **1990**, *68*, 869–874.
- (47) Toluene- d_8 was used instead of benzene- d_6 for some substrates. See the SI.
- (48) Welssman, M.; Benson, S. W. Heat of Formation of the $CHCl_2$ Radical. Bond Dissociation Energies in Chloromethanes and Chloroethanes. *J. Phys. Chem.* **1983**, *87*, 243–244.
- (49) Cioslowski, J.; Liu, G.; Moncrieff, D. Thermochemistry of Homolytic C–C, C–H, and C–Cl Bond Dissociations in Polychloroethanes: Benchmark Electronic Structure Calculations. *J. Am. Chem. Soc.* **1997**, *119* (47), 11452–11457.
- (50) Verevkin, S. P.; Krasnykh, E. L.; Wright, J. S. Thermodynamic properties of benzyl halides: enthalpies of formation, strain enthalpies, and carbon–halogen bond dissociation enthalpies. *Phys. Chem. Chem. Phys.* **2003**, *5* (12), 2605–2611.
- (51) Hori, Y.; Murata, K.; Oku, T. Electrochemical Dechlorination of Chlorinated Hydrocarbons – Electrochemical Reduction of Chloroform in Acetonitrile/Water Mixtures at High Current Density. *Chem. Lett.* **2003**, *32* (3), 230–231.
- (52) Appendix B: Tables of Physical Data. In *Fundamentals and Applications of Organic Electrochemistry: Synthesis, Materials, Devices*, 1st ed., Fuchigami, T.; Atobe, M.; Inagi, S.; John Wiley & Sons, 2015.
- (53) de Souza, R. F. M.; Laurent, M.; Léonel, E.; Cachet-Vivier, C.; de Souza, C. A.; Areias, M. C. C.; Bieber, L. W.; Navarro, M. Electrochemical Reduction of Benzyl Chloride on Silver Graphite and Silver/Graphite Powder Macroelectrodes. *Electrochim. Acta* **2015**, *167*, 105–111.
- (54) Luo, Y.-R. *Comprehensive Handbook of Chemical Bond Energies*; CRC Press: Boca Raton, 2007.
- (55) Škaič, D.; Zipse, H. Radical Stability as a Guideline in C–H Amination Reactions. *Adv. Synth. Catal.* **2016**, *358* (24), 3983–3991.
- (56) Nonhebel, D. C. The Chemistry of Cyclopropylmethyl and Related Radicals. *Chem. Soc. Rev.* **1993**, *22*, 347–359.
- (57) Newcomb, M. Radical Kinetics and Clocks. In *Encyclopedia of Radicals in Chemistry, Biology and Materials*; John Wiley & Sons, Ltd, 2012.
- (58) Ueda, M.; Doi, N.; Miyagawa, H.; Sugita, S.; Takeda, N.; Shinada, T.; Miyata, O. Reaction of Cyclopropenes with a Trichloromethyl Radical: Unprecedented Ring-Opening Reaction of Cyclopropenes with Migration. *Chem. Commun.* **2015**, *51*, 4204–4207.
- (59) Doi, N.; Takeda, N.; Miyata, O.; Ueda, M. Regiodivergent Ring-Opening Reaction of Trichloromethylcyclopropane Carboxylates. *J. Org. Chem.* **2016**, *81* (17), 7855–7861.
- (60) Sazonov, P. K.; Artamkina, G. A.; Beletskaya, I. P. Nucleophilic Substitution at the Halogen Atom (Halogenophilic Reactions). *Russ. Chem. Rev.* **2012**, *81* (4), 317–335.
- (61) Alonso, F.; Beletskaya, I. P.; Yus, M. Metal-Mediated Reductive Hydrodehalogenation of Organic Halides. *Chem. Rev.* **2002**, *102*, 4009–4091.
- (62) Farmery, K.; Kilner, M. Substitution Reactions of Dihydridotetracarbonyliron. *J. Chem. Soc. A* **1970**, 634–639.
- (63) LaCroce, S. J.; Menard, K. P.; Cutler, A. R. Reactivity Modes of Bridged Bimetallic $[\eta^5-C_5H_5]_2Fe(CO)]_2-\mu-dppe$ with Electrophiles. Preparation and Reactions of Bimetallic Hydride Complexes. *J. Organomet. Chem.* **1980**, *190*, C79–C83.
- (64) Green, M. L. H.; Wong, L.-L. η -Benzenebis(trimethylphosphine)iron as a Precursor to $Fe(\eta-C_5R_5)(PMe_3)_2$ Derivatives, $R = H, Me$: The Equilibrium $[Fe](PMe_3)Et \rightleftharpoons [Fe](\eta-C_2H_4)H + PMe_3$, where $[Fe] = Fe(\eta-C_5Me_5)(PMe_3)$. *J. Chem. Soc., Chem. Commun.* **1984**, 1442–1443.
- (65) Green, M. L. H.; Wong, L.-L. η -Benzenebis(trimethylphosphine)iron as a Precursor to $[Fe(\eta-C_5R_5)(PMe_3)_2]$ ($R = H$ or Me) Derivatives: The Equilibrium $[Fe](PMe_3)Et \rightleftharpoons [Fe](\eta-C_2H_2)H + PMe_3$, where $[Fe] = Fe(\eta-C_5Me_5)(PMe_3)$. *J. Chem. Soc., Dalton Trans.* **1987**, 411–416.
- (66) Hogarth, G.; Lavender, M. H.; Shukri, K. Diiron–Hydride Complexes: Synthesis, Structure, and Reactivity of trans- $[Fe_2(CO)_4(\mu-H)(\mu-CO)(\mu-PCy_2)(\mu-Ph_2PCH_2PPh_2)]$. *Organometallics* **1995**, *14*, 2325–2341.
- (67) Böttcher, H.-C.; Graf, M.; Merzweiler, K.; Wagner, C. Coordinatively Unsaturated Complexes $[M_2(CO)_4(\mu-H)(\mu-P^tBu_2)(\mu-Ph_2PCH_2PPh_2)]$ ($M = Fe, Ru$): Synthesis and Crystal Structures of $[Fe_2(CO)_4(\mu-H)(\mu-SO)(\mu-P^tBu_2)(\mu-Ph_2PCH_2PPh_2)]$ and $[Ru_2(CO)_4(\mu-H)(\mu-SO_2)(\mu-P^tBu_2)(\mu-Ph_2PCH_2PPh_2)]$. *Inorg. Chim. Acta* **2003**, *350*, 399–406.

- (68) Kukis, I.; Baird, M. C. Formation and Chemistry of the Transient 17-Electron Compounds $\text{CpFe}(\text{CO})\text{L}$ ($\text{L} = \text{PMe}_2\text{Ph}$, PPh_3). *J. Organomet. Chem.* **1997**, *527*, 137–143.
- (69) Yoshimoto, K.; Yatabe, T.; Matsumoto, T.; Tran, V.-H.; Robertson, A.; Nakai, H.; Koichiro Asazawa, K.; Tanaka, H.; Ogo, S. Inorganic Clusters with a $[\text{Fe}_2\text{MoOS}_3]$ Core—A Functional Model for Acetylene Reduction by Nitrogenases. *Dalton Trans.* **2016**, *45*, 14620–14627.
- (70) Birk, R.; Berke, H.; Huttner, G.; Zsolnai, L. Oxidative Addition an Tetrakoordinierte Eisenfragmente. *Chem. Ber.* **1988**, *121*, 1557–1564.
- (71) Rummelt, S. M.; Peterson, P. O.; Zhong, H.; Chirik, P. J. Oxidative Addition of Aryl and Alkyl Halides to a Reduced Iron Pincer Complex. *J. Am. Chem. Soc.* **2021**, *143*, 5928–5936.
- (72) Mendehhall, G. D.; Golden, D. M.; Benson, S. W. Thermochemistry of the Bromination of Carbon Tetrachloride and the Heat of Formation of Carbon Tetrachloride. *J. Phys. Chem.* **1973**, *77* (22), 2707–2709.
- (73) Lee, Y. R.; Yang, Y. J.; Lin, Y. Y.; Lin, S. M. Photodissociation of CBrCl_3 at 193 nm by translational spectroscopy. *J. Phys. Chem.* **1995**, *103*, 6966–6972.
- (74) Stimson, R. E.; Shriver, D. F. Lewis Basicity, Reactivity, and Bond Order of Metal Acetyls. Boron and Aluminum Halide Adducts of $(\eta\text{-C}_5\text{H}_5)\text{Fe}(\text{CO})_2(\text{C}(\text{=O})\text{CH}_3)$. *Inorg. Chem.* **1980**, *19* (5), 1141–1145.
- (75) Horwits, C. P.; Shriver, D. F. C- and O-Bonded Metal Carbonyls: Formation. Structures. and Reactions. *Adv. Organomet. Chem.* **1984**, *23*, 219–305.
- (76) Dange, D.; Sindlinger, C. P.; Aldridge, S.; Jones, C. Boryl Substituted Group 13 Metallylenes: Complexes with an Iron Carbonyl Fragment. *Chem. Commun.* **2017**, *53*, 149–152.
- (77) Richmond, T. G.; Basolo, F.; Shriver, D. F. Interaction of Metal Carbonyl Hydrides with Lewis Acids. *Organometallics* **1982**, *1*, 1624–1628.
- (78) Lee, Y.; Peters, J. C. Silylation of Iron-Bound Carbon Monoxide Affords a Terminal Fe Carbyne. *J. Am. Chem. Soc.* **2011**, *133*, 4438–4446.
- (79) Singh, D.; Knight, B. J.; Catalano, V. J.; García-Serres, R.; Maurel, V.; Mouesca, J.-M.; Murray, L. J. Partial Deoxygenative CO Homocoupling by a Diiron Complex. *Angew. Chem., Int. Ed.* **2023**, *62* (41), No. e202308813.
- (80) Nagelski, A. L.; Fataftah, M. S.; MacMillan, S. N.; MacLeod, K. C.; McWilliams, S. F.; Mercado, B. Q.; Lancaster, K. M.; Holland, P. L. Bridging Carbonyl and Carbyne Complexes of Weak-Field Iron: Electronic Structure and Iron–Carbon Bonding. *J. Am. Chem. Soc.* **2024**, *146*, 32415–32430.
- (81) Stoy, A.; Böhnke, J.; Jiménez-Halla, J. O. C.; Dewhurst, R. D.; Thiess, T.; Braunschweig, H. CO_2 Binding and Splitting by Boron–Boron Multiple Bonds. *Angew. Chem., Int. Ed.* **2018**, *57* (20), 5947–5951.
- (82) Saalfrank, C.; Fantuzzi, F.; Kupfer, T.; Ritschel, B.; Hammond, K.; Krummenacher, I.; Bertermann, R.; Wirthensohn, R.; Finze, M.; Schmid, P.; Engel, V.; Engels, B.; Braunschweig, H. cAAC-Stabilized 9,10-diboraanthracenes—Acenes with Open-Shell Singlet Biradical Ground States. *Angew. Chem., Int. Ed.* **2020**, *59* (43), 19338–19343.
- (83) Stoy, A.; Härterich, M.; Dewhurst, R. D.; Jiménez-Halla, J. O. C.; Endres, P.; Eybelein, M.; Kupfer, T.; Deissenberger, A.; Thiess, T.; Braunschweig, H. Evidence for Borylene Carbonyl ($\text{LHB}=\text{C}=\text{O}$) and Base-Stabilized ($\text{LHB}=\text{O}$) and Base-Free Oxoborane ($\text{RB}\equiv\text{O}$) Intermediates in the Reactions of Diborenes with CO_2 . *J. Am. Chem. Soc.* **2022**, *144* (8), 3376–3380.
- (84) Braunschweig, H.; Dellermann, T.; Dewhurst, R. D.; Ewing, W. C.; Hammond, K.; Jiménez-Halla, J. O. C.; Kramer, T.; Krummenacher, I.; Mies, J.; Phukan, A. K.; Vargas, A. Metal-Free Binding and Coupling of Carbon Monoxide at a Boron–Boron Triple Bond. *Nat. Chem.* **2013**, *5* (12), 1025–1028.
- (85) For an example of a diboron cluster with a linear and bridging carbonyl with a high degree of electronic delocalization ($\nu = 1972$, 1984 cm^{-1}), see: Arrowsmith, M.; Böhnke, J.; Braunschweig, H.; Celik, M. Reactivity of a Dihydrodiborene with CO: Coordination, Insertion, Cleavage, and Spontaneous Formation of a Cyclic Alkyne. *Angew. Chem., Int. Ed.* **2017**, *56* (45), 14287–14292.
- (86) Malhotra, K. C.; Sharma, N.; Bhatt, S. S.; Chaudhry, S. C. Preparation and Characterization of Monochlorotris(4-tertbutylphenoxy)titanium(IV). *Polyhedron* **1992**, *11* (16), 2065–2068.
- (87) Park, Y. L.; Ryu, J. Y.; Hwang, S.; Park, K. H.; Lee, J. M.; Cho, S.; Lee, S.; Saha, M. L.; Stang, P. S.; Lee, J. Cationic Ti Complexes with Three $[\text{N},\text{O}]$ -Type Tetrazolyl Ligands: $\text{Ti}\leftrightarrow\text{Fe}$ Transmetalation within Fe Metallascorpionate Complexes. *Inorg. Chem.* **2017**, *56*, 14060–14068.
- (88) Mono- and diformate triiron hydride complexes **7** and **8** exhibited similar thermal and photochemically stability; see Figure S54
- (89) Evans, D. F. The Determination of the Paramagnetic Susceptibility of Substances in Solution by Nuclear Magnetic Resonance. *J. Chem. Soc.* **1959**, 2003–2005.
- (90) Bain, G. A.; Berry, J. F. Diamagnetic Corrections and Pascal's Constants. *J. Chem. Educ.* **2008**, *85*, 532–536.
- (91) Sur, S. K. Measurement of Magnetic Susceptibility and Magnetic Moment of Paramagnetic Molecules in Solution by High-Field Fourier Transform NMR Spectroscopy. *J. Magn. Reson.* **1989**, *82*, 169–173.
- (92) Schubert, E. M. Utilizing the Evans Method with a Superconducting NMR Spectrometer in the Undergraduate Laboratory. *J. Chem. Educ.* **1992**, *69*, 62.
- (93) Garcia-Serres, R. *EasyMoss: A Python/PyQt5 User-Friendly Application for the Simulation of Mössbauer Spectra*; Zenodo, 2021.